EFFECT OF SEVOFLURANE ON MIGRATION AND INVASION OF CERVICAL CANCER CELLS IN RATS BY REGULATING HIPPO-YAP/TAZ SIGNALING

M. K. Fang, L. Chen and S. Q. Lu*

Department of Anesthesiology, Hubei Cancer Hospital, Wuhan, 430079, Hubei, China.
*Corresponding author's Email: shqianglu@yeah.net

ABSTRACT

This research set out to explore how sevoflurane anesthesia modulates the migratory and invasive capacities of cervical cancer cells in rats through the regulation of the Hippo-YAP/TAZ signaling pathway, providing experimental evidence for optimizing anesthetic management in cervical cancer surgery. One hundred female Sprague-Dawley rats were randomly divided into the five groups (n=20 per group): Control group (no intervention), SEV group (2% sevoflurane+1×10^6 HeLa cells), N-SEV group (4% isoflurane +1×10^6 HeLa cells), BAY593 group (4% isoflurane +10 mg/kg BAY593+1×10^6 HeLa cells), and SEV+BAY593 group (2% sevoflurane+10 mg/kg BAY593+1×10^6 HeLa cells). The tumor volume was monitored; Transwell and wound healing tests were carried out to evaluate cell invasion and migration respectively; and RT-PCR, ELISA, and Western blotting were adopted to detect the expression of pathway-related molecules. On postoperative day 28, the tumor volume in the SEV group (1.75±0.22 cm^3) was significantly larger than that in the BAY593 group (0.65±0.12 cm^3) ($P \leq 0.001$). Compared with the N-SEV group, the SEV group experienced marked body weight loss alongside prominent tumor enlargement. Meanwhile, tissue levels of YAP, TAZ, and Vimentin at both protein and transcript levels were markedly elevated, while p-YAP and E-cadherin protein abundances were substantially suppressed. Cell migration rate and the number of invasive cells were also significantly increased ($P \leq 0.05$). Relative to the SEV group, animals receiving combined SEV + BAY593 treatment displayed obvious shrinkage of tumor lesions, alleviated body weight decline, remarkable suppression of YAP, TAZ, and Vimentin levels, restored p-YAP and E-cadherin abundance, as well as robustly restrained cell migration and invasion capacity ($P \leq 0.05$). No obvious disparities were detected between the SEV + BAY593 group and the N-SEV group regarding tumor volume, cell migration rate, invasive cell count, or the abundance of all core molecular markers ($P > 0.05$). Sevoflurane anesthesia can significantly boost the migratory capacity, invasive potential and neoplastic proliferation of cervical carcinoma cells derived from rats by activating the Hippo-YAP/TAZ signaling pathway. Treatment with the YAP/TAZ pathway inhibitor BAY593 effectively blocks this effect and completely reverses the tumor-promoting effect of sevoflurane. These findings suggest that, in cervical cancer surgery, intervention targeting this pathway or selection of an alternative anesthesia regimen may help optimize anesthesia management and improve prognosis.

Keywords: sevoflurane; cervical cancer; Hippo-YAP/TAZ pathway; tumor volume; migration

This article is an open access article distributed under the terms and conditions of the Creative Commons Attribution (CC BY) license (https://creativecommons.org/licenses/by/4.0

Received January 11, 2026 Published Online October 21, 2026 https://doi.org/10.36899/JAPS.2027.1.0006

INTRODUCTION

Cervical malignancy is a cause of poor prognosis and treatment failure in oncology. With the recent continuous development of health technology, some promising results have begun to be shown in the treatment of cervical cancer. Despite these issues, management of advanced cervical cancer is still hindered by several factors due to the presence of tumour metastasis, including a high recurrence rate, treatment resistance, and a low overall survival rate for patients (Das *et al.*, 2023; Bou Antoun *et al.*, 2025). Migration and invasion of tumour cells are the first two links in the metastatic chain (Novikov *et al.*, 2021). Therefore, the whole system of regulation should be known in order to adjust the course of treatment for patients.

Although surgery is generally the first way to treat cervical cancer, over time, anaesthetic agents and related perioperative factors have been found to modulate cancer cell proliferation at the basic level (Ishikawa *et al.*, 2021; Fan *et al.*, 2020). Sevoflurane is widely used in clinical anaesthesia owing to its minimal blood-gas distribution ratio and rapid induction and emergence (Yang *et al.*, 2024). This agent causes various changes in the body of patients under general anaesthesia and may also alter the biological traits of tumours by modifying cellular pathways. Some scholars have found that sevoflurane can suppress the multiplication and metastasis of malignant cells via inhibiting the Wnt/β-

catenin signalling pathway and regulating the PI3K/Akt cascade. (Cao *et al.*, 2020; Chen *et al.*, 2019). Based on the above studies, Sevoflurane has been associated with the growth of tumours and the spread of lung metastases in ovarian cancer (Hu *et al*., 2024). Therefore, it can be assumed that the effect of sevoflurane on tumours may be restricted to certain tissues or pathways, and the exact reasons are not yet known.

The Hippo-YAP/PDZ-binding motif (PABM) transcriptional coactivator pathway is one of the factors that control the size and shape of organs and tissues based on both inside and outside stimuli; Recently, it has also been found that this pathway promotes the development and spread of cervical cancer. Hippo-YAP/TAZ signaling regulates various cell activities and acts imperatively in cervical cancer initiation and progression (Patterson *et al*., 2024). Hippo-YAP/TAZ signaling was discovered through genetic studies in Drosophila melanogaster, regulating organ size and tissue growth (Pan, 2022). The main signalling path is as follows: MST1/2 kinases catalyze phosphorylation and trigger activation of LATS1/2, which then directly phosphorylates YAP/TAZ to block their nuclear entry and accelerate their proteolytic breakdown. In normal cells, the Hippo pathway maintains cellular homeostasis, regulates the size of organs, suppresses excessive proliferation, and promotes apoptosis by inhibiting YAP/TAZ. Impairment of the Hippo signalling network can result in dephosphorylation and nuclear accumulation of YAP/TAZ; these proteins subsequently interact with the TEAD family of transcription factors to upregulate gene expression driving cell growth, repressing cell death, and boosting metastatic potential, such as CTGF and CYR61. Previous research has shown that the dysregulated activation of YAP/TAZ is involved in the malignant progression of cervical cancer, and HIF-1α can stimulate proliferative activity, migratory capacity and invasive properties of cervical cancer cells via elevating YAP/TAZ expression (Abudoukerimu *et al.*, 2022). YAP/TAZ may also promote epithelial-mesenchymal transition (EMT) through boosting transcriptional output of EMT-triggering molecules such as Snail, Twist and ZEB1, and meanwhile downregulate E-cadherin levels and raise Vimentin abundance to support the movement of neoplastic cells (Zhou *et al.*, 2023; Choi *et al.*, 2024). At the same time, the Hippo-YAP/TAZ axis also crosstalks with signalling pathways such as PI3K/Akt and GPCR, collectively regulating cellular behaviours within the tumour microenvironment. Accordingly, therapeutic intervention against this signalling cascade offers an alternative treatment approach for cervical cancer.

Although Sevoflurane exerts influence on malignancies via diverse mechanisms, its specific impact on the metastatic behavior of cervical carcinoma cells through the Hippo-YAP/TAZ axis is still undefined. According to existing research, sevoflurane suppresses oncogenic cell expansion and motility by adjusting intracellular signaling cascades (Ishikawa *et al*., 2021); Meanwhile, the Hippo-YAP/TAZ signaling pathway is considered to be an important molecular axis that regulates tumor cell migration and metastatic potential (Fan *et al*., 2020). Given this background, we propose that sevoflurane anesthesia might facilitate the spread and infiltration of cervical tumor cells by triggering the Hippo-YAP/TAZ signaling network. To verify this hypothesis, immunosuppressed rats were selected because of their large size, which is convenient for blood collection, ultrasound examination and tissue collection, and HeLa cells were employed due to their good tumorigenicity, pathway sensitivity and stability. Immunosuppression was induced using cyclophosphamide rather than employing nude rats, as nude rats are immunodeficient and costly, whereas the cyclophosphamide model more closely mimics the perioperative immunosuppressive state observed in clinical settings. The goal was to provide new insights into anesthetic drugs' role in tumor cell migration and metastasis, while offering novel perspectives for therapeutic strategies in cervical cancer.

MATERIALS AND METHODS

Cell line culture: The human cervical carcinoma HeLa cell line (American Type Culture Collection, USA) was employed as the experimental material in the present investigation. Logarithmically growing HeLa cells were maintained in RPMI-1640 culture medium supplemented with 10% FBS and 1% penicillin/streptomycin mixture; the stock solution, which contained 10,000 U/mL penicillin and 10 mg/mL streptomycin, was prepared through 1:100 dilution (Thermo Fisher, USA). The incubator was set to 37°C, with 95% relative humidity and 5% CO_2 concentration (Thermo Fisher, USA). When the cells are approximately 80%-90% confluent, wash them with 0.25% trypsin (Trypsin-EDTA; Thermo Fisher, USA) one time and then collect the cells. At the start of digestion, the first medium was removed, and then once washed with calcium- and magnesium-free PBS (Thermo Fisher, USA) to wash away any remaining medium. Trypsin solution was then applied to incubate cells at 37°C for 2-3 minutes until fully dispersed. Cell status was monitored under a microscope (Model: Olympus IX73; Olympus, Japan), and once complete detachment was confirmed, equivalent amounts of complete culture medium were added to terminate the digestion process. After digestion, cell numbers were counted employing a cell counting chamber (Thermo Fisher, USA), and the cellular concentration was calibrated to 1×10^6 cells/mL.

Animals: One hundred female Sprague-Dawley rats (weighing approximately 200-250 g and aged 8-10 weeks) were obtained (Shanghai SLAC Laboratory Animal Co., Ltd., China). Compared with the previous mouse model, the rat has a

relatively mild cervical area suitable for local injection and high-frequency ultrasound observation, and is in good condition for bearing multiple stages of anaesthesia and blood collection over 28 days. Preliminary experiments have shown that the rate of tumour development in immunodepressed rats (about 85%) is close to that in nude mice (about 90%), and the pattern of tumour growth is also more uniform. All of the rats were kept in the lab before the start of the experiment and allowed to settle for 7 days. At that time, the animals were housed under conditions of 22±2°C, relative humidity of 50-60%, and a 12-hour light/dark cycle (with the light phase occurring from 6:00-18:00). The animals were provided with regular laboratory animal food (Beijing Keao Xieli Animal Technology Co., Ltd., China) and clean tap water ad libitum, ensuring adequate supply of both food and water under sterile conditions. All the animals' cages were equipped with a standard ventilation system to maintain air quality. Three to five rats per cage were kept to ensure socialisation and good health. To create an immunosuppressive environment for xenografting human-derived tumor cells, rats were intraperitoneally administered cyclophosphamide (Sigma-Aldrich, USA) at 50 mg/kg, 3 days before tumor cell introduction and on the day of introduction to inhibit immune system responses. Based on the initial experimental data, a suitable dosage and schedule for administering cyclophosphamide were selected to achieve good immunosuppression while avoiding excessive toxicity. At the same time, the activity and behavior of all the rats were closely monitored during the experiment to ensure no signs of stress or abnormal behavior. Non-invasive methods were employed to measure the rats' body weight and overall health status. In all experiments involving animals, the purpose of reducing pain and minimising the number of animals used in line with the 3R principles (Replacement, Reduction and Refinement) was realised. The hospital's Ethics Committee provided ethical approval for the present study, which complies with the requirements of China's National Animal Utilisation Standards and ARRIVE 2.0 publication guidelines.

Grouping and treatments: The rodents were stochastically divided into five groups (n=20 in each group). During the monitoring of tumour volume by ultrasound, behavioural observation and subsequent statistical analysis, all researchers remained blinded to the grouping information to minimize measurement bias. The different interventions for each group were as follows:

Control group: Rats did not receive HeLa cell injection, anaesthesia or surgery. They acted as blank controls to establish the baseline state for any intervention and provided a source of normal cervical tissue for basic molecular measurements.

Non-SEV group (N-SEV group): To control for the effects of the inhalation anaesthesia procedure itself and surgical stress, rats in this group received isoflurane anaesthesia before the injection of cervical cancer cells. The rodents were transferred into an induction box and inhaled 4% isoflurane at an oxygen delivery rate of 2 L/min over a 5-minute period. Following disappearance of the righting reflex, continuous anaesthesia was sustained using 2% isoflurane (flow rate 0.3–0.5 L/min) administered via the nasal route for approximately 15–20 minutes, with the concentration adjusted to ensure no response to surgical stimulation. Once anaesthesia was stabilized, 1×10^6 HeLa cells (in a suspension volume ≤ 50 μL) were injected into the cervical submucosa through a 30 G needle to establish a tumour model. This group was utilized to account for impacts caused by the surgical procedure and background anaesthesia itself, and served as the benchmark for evaluating the sevoflurane-specific effects.

Sevoflurane group (SEV group): Sevoflurane (Abbott Laboratories, USA) was used to induce sedation in the animals before the injection of cervical cancer cells. The rat was put in a special induction chamber, and 5% sevoflurane was given (oxygen flow 2L/min) for 5 minutes, and then the righting reflex disappeared. Then, 2% sevoflurane was given through the nose at a flow rate of 0.3~0.5 L/min; sedation was maintained, and at this time, breathing, heart rate, and paw-pinch sensation were observed every 5 minutes. The sevoflurane concentration was maintained within the range of 1.8%-2.2% as required to ensure no response to surgical stimuli. The total anesthesia duration was approximately 15-20 minutes, and all rats regained consciousness within 10 minutes after injection. Continuous monitoring using a physiological monitor ensured oxygen saturation >95%, heart rate of 300-450 beats/min, and respiratory rate of 60-80 breaths/min; in cases of respiratory depression, the sevoflurane concentration was immediately reduced to 1.5%, and pure oxygen was administered. After anesthesia, cells were inoculated by cervical injection. The cell suspension was diluted in PBS (Thermo Fisher, USA) to an appropriate concentration (1×10^6 cells per rat) and injected submucosally into the cervix. Each rat was inoculated with approximately 1×10^6 HeLa cells.

Hippo-YAP/TAZ inhibition group (BAY593 group): Rats were maintained under isoflurane background anesthesia (4% concentration, oxygen flow rate 2 L/min; 2% via nasal mask at 0.3–0.5 L/min for 15–20 min), they were inoculated with 1×10^6 HeLa cervical cancer cells as in the SEV group, while simultaneously receiving intraperitoneal injections of a Hippo-YAP/TAZ signaling inhibitor (BAY593, Sigma-Aldrich, USA) at 10 mg/kg, administered every 2 days until the end of the experiment.

SEV+Hippo - YAP/TAZ inhibition group (SEV+BAY593 group): Rats in this group were anesthetized with sevoflurane (concentration 2%) before cervical injection of 1×10^6 HeLa cells. Concurrently, they received intraperitoneal injections of a Hippo-YAP/TAZ signaling inhibitor (BAY593, dose 10 mg/kg, every 2 days).

All rats were continuously observed for 7 days after tumor cell injection, during which body weight, health status, behavior, and physiological responses were monitored. On day 7 after cell injection, tumor formation was first screened and confirmed by high-frequency ultrasound imaging, after which formal quantitative monitoring of tumor volume was initiated once every 3 days. Tumor formation was confirmed by a well-defined hypoechoic mass at the injection site with loss of normal cervical tissue architecture; the mass was measurable in both longitudinal and transverse planes, and its volume (calculated as volume = length × width × height × π/6) exceeded 0.5 cm^3. Tumor formation was confirmed when these criteria were met on two consecutive examinations (Zaman *et al*., 2016). An operator blinded to the experimental group allocation performed ultrasound examinations.

Monitoring of tumor volume: From day 1 post-injection, cervical cancer tumor volume was monitored using high-frequency ultrasound equipment (Vevo 3100, VisualSonics, USA). Tumors were observed for 28 days and monitored daily. A high-frequency ultrasound probe (18-38 MHz) was used to conduct longitudinal and transverse scans of the tumors. The tumor's longest and shortest diameters were recorded, and its volume was computed.

Tissue collection and preparation: After completing the above research, humane euthanasia was performed on the animals by CO2 asphyxiation in accordance with the 2020 AVMA Protocols for Animal Euthanasia and the recommendations of the National Institutes of Health Animal Care and Use Committee for euthanising small rodents. Next, these subjects were rapidly dissected to obtain the cervical neoplastic tissues. The tissue was split into two portions, and one segment was prepared for histological sections. Then, the samples were placed in 4% paraformaldehyde (Sigma-Aldrich, USA) for 24 hours. After fixation, the specimens were rinsed with running water to remove excess fixative, then dehydrated by a series of progressively increasing concentrations of alcohol solutions (70%–100%) (Sinopharm Chemical Reagent Co., China). Once dehydration was complete, the tissue samples were cleared in xylene (Alfa Aesar, USA) and embedded in paraffin (Thermo Fisher, USA). Paraffin blocks were cooled and solidified, then sectioned into 5 μm-thick slices utilizing a Leica RM2235 microtome (Leica Microsystems, Germany), placed on glass slides (Thermo Fisher, USA) in preparation for subsequent staining. The remaining tumour samples were used to extract proteins and RNA, as well as conduct functional cell assays. Under sterile conditions, the tissues were divided into several small portions, which were allocated for Western blotting, RNA extraction and qPCR, wound healing experiments and Transwell assays.

Primary cell isolation (for wound healing and Transwell assays): Remove the excess malignant tissue (approximately 50–100 mg according to the size of the lesion), dissect it into 1 mm^3 fragments, and then, in a 0.2% type I collagenase (Sigma-Aldrich, USA) and 0.25% trypsin-EDTA (Thermo Fisher, USA) solution, place them in a 37°C water bath and shake for 30 minutes. Filter the digested mixture through a 70 μm cell filter, collect the filtrate, and then centrifuge the filtrate at 300 × g for 5 minutes. Re-suspend the cell pellet in RPMI-1640 complete medium+10% FBS+1% penicillin-streptomycin, maintain it in a 37°C+5% CO2 incubator for 24 hours, and then move to the subsequent stage. After cell counting with Trypan blue staining, only cells with a viability of over 90% were used for subsequent wound healing and Transwell experiments. All investigations used primary tumour cells with a passage number of no more than two to maintain the biological characteristics of in vivo tumour cells.

Scratch test: Primary tumour cells were obtained from the above experimental groups. These cells were added to 6-well culture dishes containing RPMI-1640 medium supplemented with 10% FBS and 1% penicillin-streptomycin, followed by continuous cultivation until the cell monolayer reached 90–95% coverage. Afterwards, a consistent wound gap was generated across the cell sheet using a sterilized 200-μL pipette tip. After three gentle washes in sterile PBS to remove detached cells, the remaining cells were cultured in serum-free RPMI-1640 medium. Images of the scratch region at 0 and 24 hours were captured with an inverted microscope (Olympus CKX41, Japan). ImageJ software (National Institutes of Health, USA) was employed to quantify the changes in the scratch area and the percentage of wound healing.

Transwell migration assay: The migratory ability of primary tumour cells from all groups was determined by a Transwell system using polycarbonate membranes with a pore diameter of 8 μm (Corning, USA) in 24-well plates. Specifically, 1×10^5 primary tumour cells resuspended in 200 μL serum-free RPMI-1640 medium were seeded into the upper chamber. Subsequently, 600 μL RPMI-1640 medium containing 20% fetal bovine serum serving as a chemotactic stimulus was placed into the lower chamber. Place Transwell plates in a 5% CO_2 incubator at 37°C for 24 hours. Afterwards, non-invasive cells remaining on the interior face of the upper membrane were gently removed with a cotton swab. Those cells crossing over to the basal face of the membrane were fixed with 4% paraformaldehyde and stained via

0.1% crystal violet. Using an optical microscope (Olympus CX41, Japan), imaging was performed for five randomly selected visual regions within each well, followed by quantification of migrated cell populations.

ELISA: ELISA was adopted to quantify the abundance of proteins belonging to the Hippo-YAP/TAZ signal cascade and other metastasis-associated mediators within cervical cancer tissue samples. First, approximately 50 mg of solid cervical tumour tissue was thawed, fragmented and lysed in NP-40 lysis buffer (Thermo Fisher, USA) containing a mixture of protease and phosphatase inhibitor agents. Homogenisation on ice was carried out with a tissue homogenizer to obtain the lysates. The homogenate was spun at 12,000×g for 15 minutes at 4°C, and the supernatant fraction was subsequently harvested. The total protein concentration was quantified through the BCA assay (Bicinchoninic Acid Assay, Thermo Fisher, USA). Then, using the above-mentioned specific kits, ELISA tests were implemented following the official protocols provided by the reagent supplier to measure YAP, TAZ, E-cadherin and Vimentin (Sigma-Aldrich, USA). Add the diluted protein extract to the 96-well plate pre-immobilized with matching capture antibody, and subsequently maintain incubation at 37°C for 2 hours. Following incubation, the plate was washed and blocked, then biotin-labelled detection antibodies were added for 1 hour at 37°C. Then wash the plate, add horseradish peroxidase-conjugated streptavidin, and maintain incubation at 37°C for 30 minutes. Finally, TMB substrate solution was dispensed into each well, and the plates were kept away from light for 15 minutes to induce colour generation; then, the stop solution was added to halt the reaction. A Thermo Fisher microplate reader (USA) was employed to measure the absorbance (optical density, OD) at 450 nm of all samples in triplicate. Based on the standard curve, the levels of all proteins (ng/mg total protein) were calculated. A solvent-only negative control and a kit-standard positive control were used to ensure the correctness of the experimental results. All the specimens were tested within the same batch to reduce inter-batch variation.

qPCR: Total cellular RNA was extracted from frozen tissue specimens using TRIzol. NanoDrop 2000 Spectrophotometer was used to measure the concentration and purity of RNA; the A260/A280 value ranged from 1.8 to 2.0. One microgram of RNA was applied for cDNA synthesis by means of the PrimeScript™ RT reagent kit. A 20 µL reaction system was assembled, composed of 10 µL of the SYBR Green master mix, 0.4 µL of each forward and reverse primer (10 µM), 1 µL of cDNA, together with nuclease-free water to reach the total reaction volume. Under these reaction parameters, the amplification process was run on a Bio-Rad CFX96 instrument: first, an initial denaturation step was held at 95°C for 10 minutes; then, 40 cycles consisting of 95°C for 15 seconds and 60°C for 30 seconds were carried out; finally, the melt curve was analysed. Primer3 was used to design primers, and then they were validated in NCBI to avoid dimer formation and non-specific amplification; the length of the product was between 100 and 200 bp. The sequence is as follows: YAP (150 bp) forward 5'-AGACGGAGTGAGGAGGAGC-3', reverse 5'-TCAGTTCTGTGTCCTCCAG-3'; TAZ (140 bp) forward 5'-TGGAGGATGAGAGGAGGAGG-3' and reverse 5'-CAGGAGGAGAGTGTTGAGG-3'; Vimentin (135 bp) forward 5'-GAGAGCGAGGAGGAGGACAG-3' and reverse 5'-GCTGGTGGCTTGAGGAAGG-3'; E-cadherin (160 bp) forward 5'-AAGGAGGAAGGAGGAGGAAG-3' and reverse 5'-GGAGGAAGAGAGAGGAGG-3'; and the internal control GAPDH (145 bp) forward 5'-ACAGTCCATGCCATCACTG-3' and reverse 5'-TGGACTCCACGACGTACTC-3'. Using the 2-ΔΔCt method, GAPDH was taken as the reference control to determine the relative abundance of YAP, TAZ, Vimentin and E-cadherin.

Western blotting: Centrifuge the cooled tissue samples, then mix and grind them, add ice-cold extraction reagent containing protease and phosphatase inhibitors (RIPA; Thermo Fisher, USA) to lyse the cells, and obtain total cellular proteins. The BCA protein quantification kit (Thermo Fisher Scientific, USA) was applied to measure the protein content. These samples were kept at -80 °C for a long time before use. Sodium dodecyl sulphate-polyacrylamide gel electrophoresis (Bio-Rad, USA) was adopted to resolve 20 µg of protein, and then, via a wet-transfer method, blotted onto polyvinylidene fluoride membranes (Millipore, USA) for 90 minutes at 100 V. Membranes were blocked in 5% non-fat milk for 60 min, followed by incubation overnight at 4°C with primary antibodies (YAP, TAZ, phosphorylated YAP (p-YAP), E-cadherin and Vimentin; each at a 1:1000 dilution) (Cell Signaling Technology, USA). Negative (no primary antibody) and positive control samples were added. On the subsequent day, the filters underwent three rinses, after which horseradish peroxidase-conjugated secondary antibody prepared at a 1:2000 dilution was supplemented and maintained for a 1-hour incubation period. ECL reagents from Thermo Fisher, USA, were used to conduct chemiluminescence imaging, and then ImageJ was employed for protein quantification. Normalise the intensity of the target protein to that of glyceraldehyde-3-phosphate dehydrogenase (GAPDH) at a ratio of 1:5000 (Sigma-Aldrich, USA). All samples were analyzed in triplicate to verify the accuracy of the data.

Statistical methods: All inference tests were carried out in SPSS 26.0 (IBM, USA). First, normality (Shapiro-Wilk test) and homogeneity of variance (Levene's test) of the continuous variables were examined. Normally distributed data with a constant variance can be expressed as Mean ± Standard Deviation (Mean ± SD). Linear mixed models (LMM) were used to examine the impact of group, time and their interaction as fixed factors, and subjects as random effects, for repeated-

measure data (body weight and tumour volume). This way is still robust to the violation of the sphericity constraint. Other single-time-point endpoint metrics were analysed using one-way ANOVA. If the results of the ANOVA showed a significant difference ($P \leq 0.05$), then Tukey's Honestly Significant Difference (HSD) test was performed for several pairwise comparisons to control the family-wise error rate. To avoid excessive inflation of Type I error due to multiple endpoints, this report focuses on the pre-specified major pairwise comparisons: (1) SEV vs. Control, (2) SEV vs. N-SEV, (3) SEV vs. SEV+BAY593, and (4) BAY593 vs. Control. Other inter-group comparisons were considered exploratory analyses. Statistical significance is set at $P \leq 0.05$.

RESULTS

Changes in body weight in rats: The changes in body weight of the rats in each experimental group over 28 consecutive days are shown in Table 1. According to the LMM results, there is a significant interaction between the length of observation and the experimental intervention ($F_{4\cdot18,\ 103\cdot6}=7.52$, $P \leq 0.001$). Initially, the five experimental groups had no significant difference in the initial body mass ($F_{4,\ 95}=0.92$, $P=0.46$). Over the 28-day treatment period, the Control group had a steady increase of +15% (95% CI: 12%-18%). Conversely, the SEV group demonstrated the greatest decline in body mass, dropping by nearly 10% (95% CI: −13% to −7%) by day 28. Tukey's HSD was used to conduct the pre-specified major pairwise comparisons, and it was found that the drop in body weight for the SEV group was significantly greater than that in the Control group (mean difference = -25%, 95% CI: -32% to -18%, $P \leq 0.001$), as well as for the N-SEV group (mean difference = -5%, 95% CI: -9% to -1%, $P \leq 0.05$) and the BAY593 group (mean difference = -8%, 95% CI: -13% to -3%, $P \leq 0.01$). In addition, the body weight reduction of the SEV+BAY593 group was significantly less than that in the SEV group (mean difference = 4%, 95% CI: 1%-7%, $P \leq 0.05$).

Table 1 Weight changes of rats in each group within 28 days (n=20, x̄±SD)

Group (each *n*=20)	Initial weight (g)	Weight on 7th day (g)	Weight on 14th day (g)	Weight on 21th day (g)	Weight on 28th day (g)	Weight change (%)
Control group	250±10	260±12	265±15	270±16	275±17	15%
SEV group	248±8	245±9	240±10	235±11	223±12	-10%
N-SEV group	252±9	250±8	245±9	240±10	232±10	-8%
BAY593 group	255±11	252±10	249±10	245±11	244±12	-2%
SEV+BAY593 group	253±9	245±10	238±11	233±10	237±11	-6%

Influence of sevoflurane on tumor volume in cervical cancer rats: LMM analysis revealed a significant time-by-group interaction effect ($F_{3\cdot92,\ 97\cdot8} = 11.86$, $P \leq 0.001$). On day 28, the tumor volume in the SEV group (1.75 ± 0.22 cm³) was significantly larger than that in the N-SEV group (1.10 ± 0.20 cm³) (mean difference = 0.65 cm³, 95% CI: 0.40 – 0.90, $P \leq 0.001$, Tukey's HSD) and the BAY593 group (0.65 ± 0.12 cm³) (mean difference = 1.10 cm³, 95% CI: 0.30–0.80, $P \leq 0.001$, Tukey's HSD). The tumor volume in the SEV+BAY593 group (1.20 ± 0.17 cm³) was significantly smaller than that in the SEV group (mean difference = −0.55 cm³, 95% CI: −0.80 to −0.30, $P \leq 0.01$, Tukey's HSD) (Figure 1).

The effect of Sevoflurane on protein expression in cervical tumor tissue of rats with cervical cancer: YAP, TAZ, Vimentin, and E-cadherin protein levels in the cervical tumor samples of rats in all groups were measured by ELISA and shown in Figure 2. Statistical analyses adopting one-way ANOVA with subsequent Tukey's HSD post-hoc assessments were implemented to carry out intergroup pairwise evaluations. The protein abundances of YAP, TAZ and Vimentin within the SEV group exhibited prominent elevation relative to the Control group (roughly 45%, 40% and 38% greater, respectively; all $P \leq 0.01$, Tukey's HSD). Compared with the N-SEV group, the protein levels in the SEV group were also significantly increased (approximately 33%, 29% and 36% higher, respectively; all $P \leq 0.05$, Tukey's post hoc test). Conversely, E-cadherin contents in the SEV group were markedly diminished (roughly 30% lower when contrasted against the Control group, $P \leq 0.001$; about 18% less than in the N-SEV group, $P \leq 0.05$, Tukey's post hoc test). Relative to the Control group, the expression quantities of YAP, TAZ and Vimentin showed obvious downregulation in the BAY593 group, whereas E-cadherin protein expression displayed remarkable upregulation (all $P \leq 0.05$, Tukey's post-hoc test). When set against the SEV group, YAP, TAZ and Vimentin protein abundances in the SEV + BAY593 group were substantially decreased (by about 30%, 31% and 30% respectively; all $P \leq 0.05$, Tukey's post hoc test), while E-cadherin protein levels were substantially boosted (by about 34%, $P \leq 0.01$, Tukey's post hoc test).

Influence of sevoflurane on cell migration in cervical cancer rats: To evaluate the migration ability of cervical cancer cells, a scratch assay was used (Fig. 3). The wound healing rates in the Control, SEV, N-SEV, BAY593, and

SEV+BAY593 groups were 13.12±3.29%, 59.23±6.33%, 35.45±5.29%, 16.02±3.11%, and 36.55±6.77%, respectively. A single-factor ANOVA found a significant difference among the groups ($F_{4,\ 95}$ = 32.18, $P \leq 0.001$). Using Tukey's HSD for the pre-specified main comparisons, it was found that the cell migration rate in the SEV group was significantly higher than that in the Control group (mean difference = 46.11%, 95% CI: 38.5%–53.7%, $P \leq 0.001$), and similarly, it was higher than that in the N-SEV group (mean difference = 23.78%, 95% CI: 16.2%–31.4%, $P \leq 0.01$). The migration rate of the SEV+BAY593 group was significantly lower than that of the SEV group (mean difference = -22.68%, 95% CI: -31.2% to -14.2%, $P \leq 0.01$, Tukey's HSD). Additionally, the migration rate of the BAY593 group was also significantly lower than that in the Control group (mean difference = -16.02%, 95% CI: -24.6% to -7.4%, $P \leq 0.05$, Tukey's HSD).

Changes in invasion ability of tumor cells: Different interventions yielded distinct regulatory outcomes on the invasive capacity of cervical cancer cells as verified by Transwell assays (Figure 4). The numbers of invasive cells in the Control, SEV, N-SEV, BAY593, and SEV+BAY593 groups were 138.12±29.29, 254.19±35.12, 200.33±33.22, 140.33±33.11, and 196.39±24.98, respectively. One-way ANOVA showed that the five groups were significantly different ($F_{4,\ 95}$ = 20.85, $P \leq 0.001$). Using Tukey's HSD test to conduct the pre-specified major pairwise comparisons, the results demonstrated that the SEV group possessed a markedly increased quantity of infiltrative cells compared with the Control group (mean difference = 116.07, 95% CI: 78.5–153.6, $P \leq 0.001$) and the N-SEV group (mean difference = 53.86, 95% CI: 16.3–91.4, $P \leq 0.05$). The SEV+BAY593 group presented a prominently decreased number of invasive cells relative to the SEV group (mean difference = -57.80, 95% CI: -95.3 to -20.3, $P \leq 0.01$, Tukey's HSD). No statistically notable discrepancy existed between the BAY593 group and the Control group in terms of invasive cell counts (mean difference = 2.21, 95% CI: -35.2 to 39.6, $P = 0.97$).

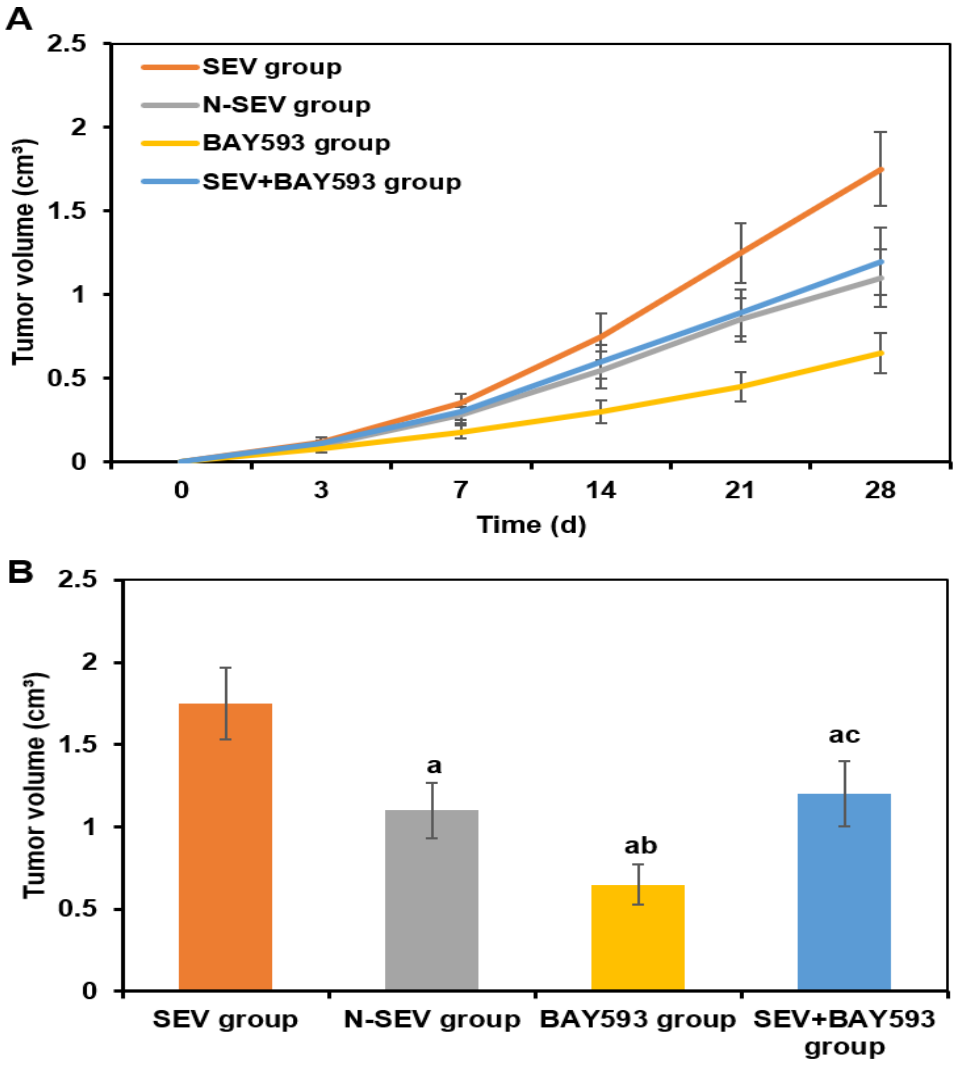
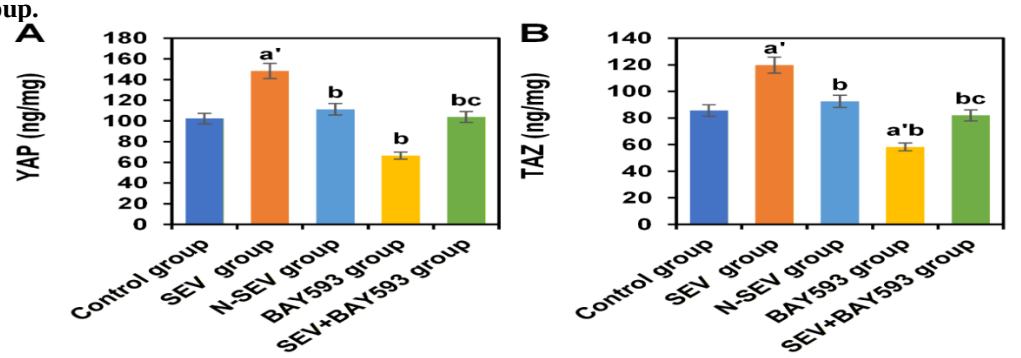


Figure 1. Contrast of cervical tumor volume monitoring results in rats from different groups (mean±SD). The error line was the standard deviation. A: tumor changes from day 0 to day 28; B: comparison of tumor volume among groups on day 28. [a]*P*≤0.05 vs. SEV group; [b]*P*≤0.05 vs. N-SEV group; [c]*P*≤0.05 vs. BAY593 group.



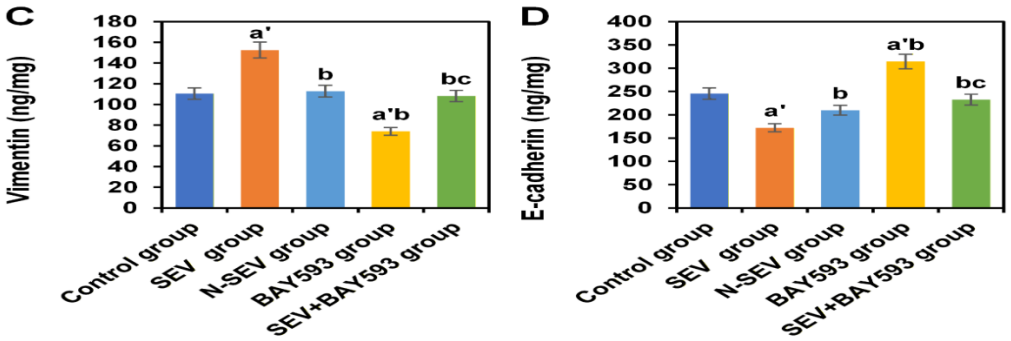


Figure 2. ELISA assay results for each group (mean±SD). Error bars represent standard deviation. A: Comparison of YAP protein levels; B: Comparison of TAZ protein levels; C: Comparison of Vimentin protein levels; D: Comparison of E-cadherin protein levels. [a']*P*≤0.05 vs. Control group; [b]*P*≤0.05 vs. SEV group; [c]*P*≤0.05 vs. BAY593 group.

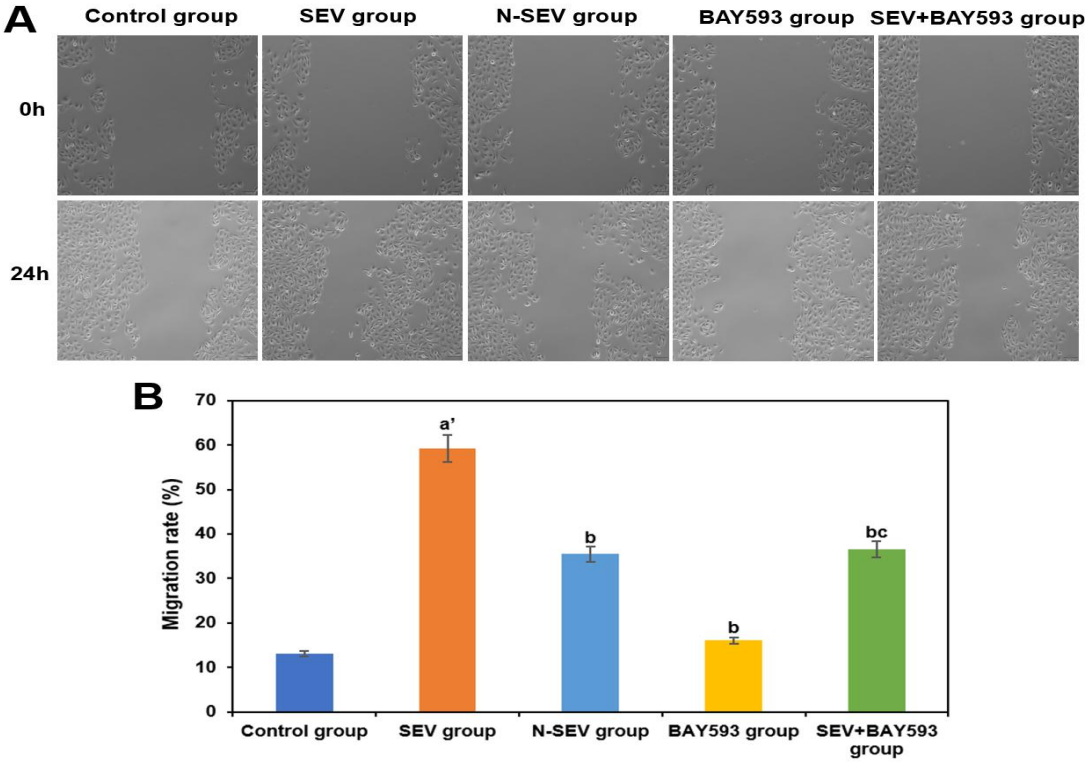


Figure 3. Scratch assay results for each group (mean±SD). The error line was the standard deviation. A: representative images of the scratch assay; B: comparison of cell migration rates among groups. [a']*P*≤0.05 vs. Control group; [b]*P*≤0.05 vs. SEV group; [c]*P*≤0.05 vs. BAY593 group.

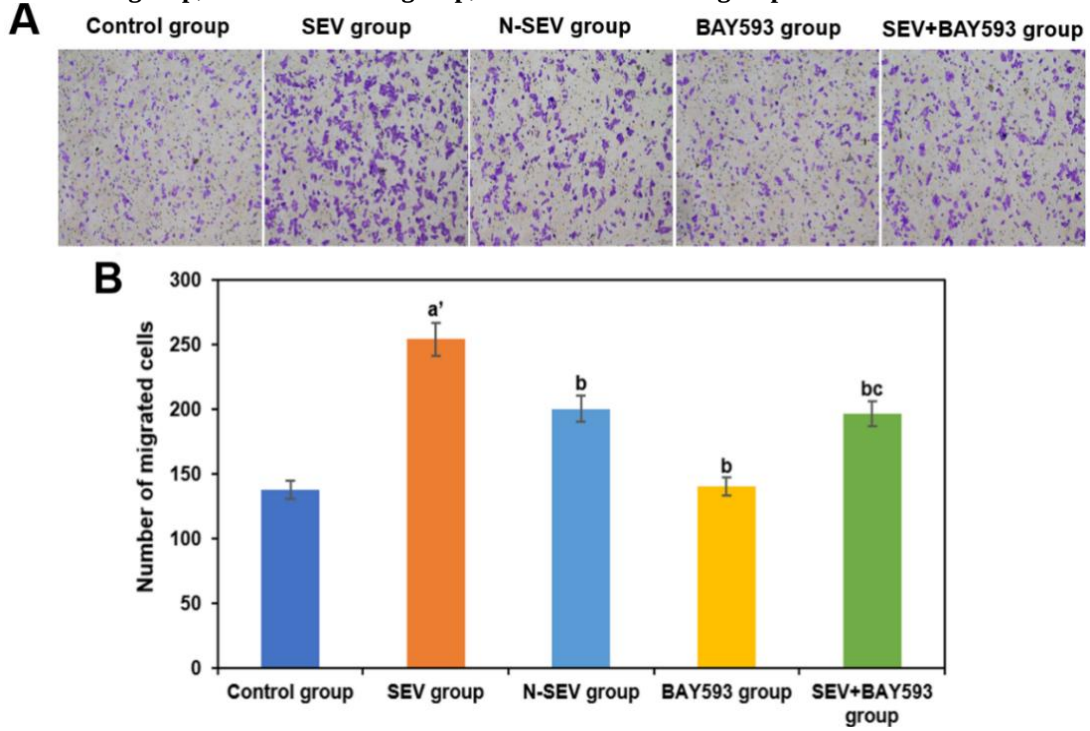
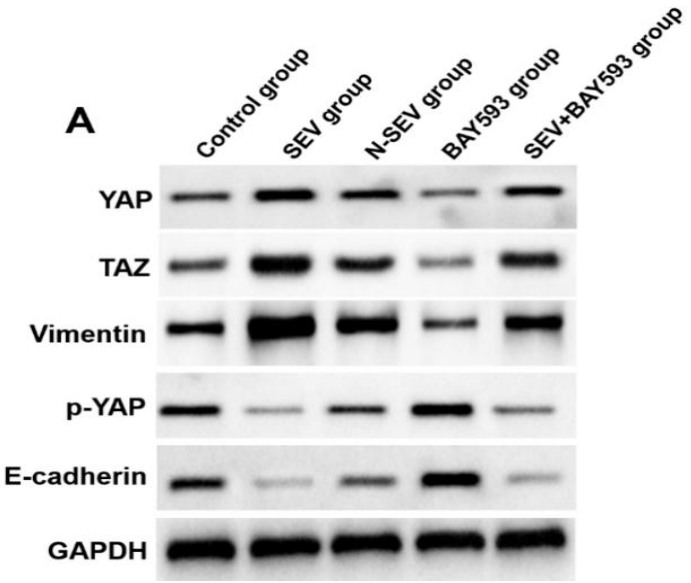


Figure 4. Transwell assay results for each group (mean±SD). The error line was the standard deviation. A: Representative images of the Transwell assay. B: Comparison of the number of migrated cells among groups. [a']*P*≤0.05 vs. Control group; [b]*P*≤0.05 vs. SEV group; [c]*P*≤0.05 vs. BAY593 group.

Expression changes of key proteins in the YAP/TAZ pathway: The results of Western Blot and qPCR analyses are shown in Figure 5. At both protein and mRNA levels, one-way ANOVA revealed significant differences among all groups for all indicators (all $P \leq 0.001$). Compared with the Control group, the SEV group had significantly increased protein and mRNA levels of YAP, TAZ and Vimentin (all $P \leq 0.01$, Tukey's HSD), as well as significantly higher levels than the N-SEV group (all $P \leq 0.05$, Tukey's HSD), but p-YAP and E-cadherin were significantly reduced (all $P \leq 0.05$, Tukey's HSD). Compared with the SEV group, the SEV+BAY593 group had significantly lower YAP, TAZ and Vimentin at both the protein and mRNA levels (all $P \leq 0.05$, Tukey's HSD), and significantly increased p-YAP and E-cadherin. The BAY593 group showed the most pronounced reversal of molecular changes compared with the Control group (all $P \leq 0.05$, Tukey's HSD).



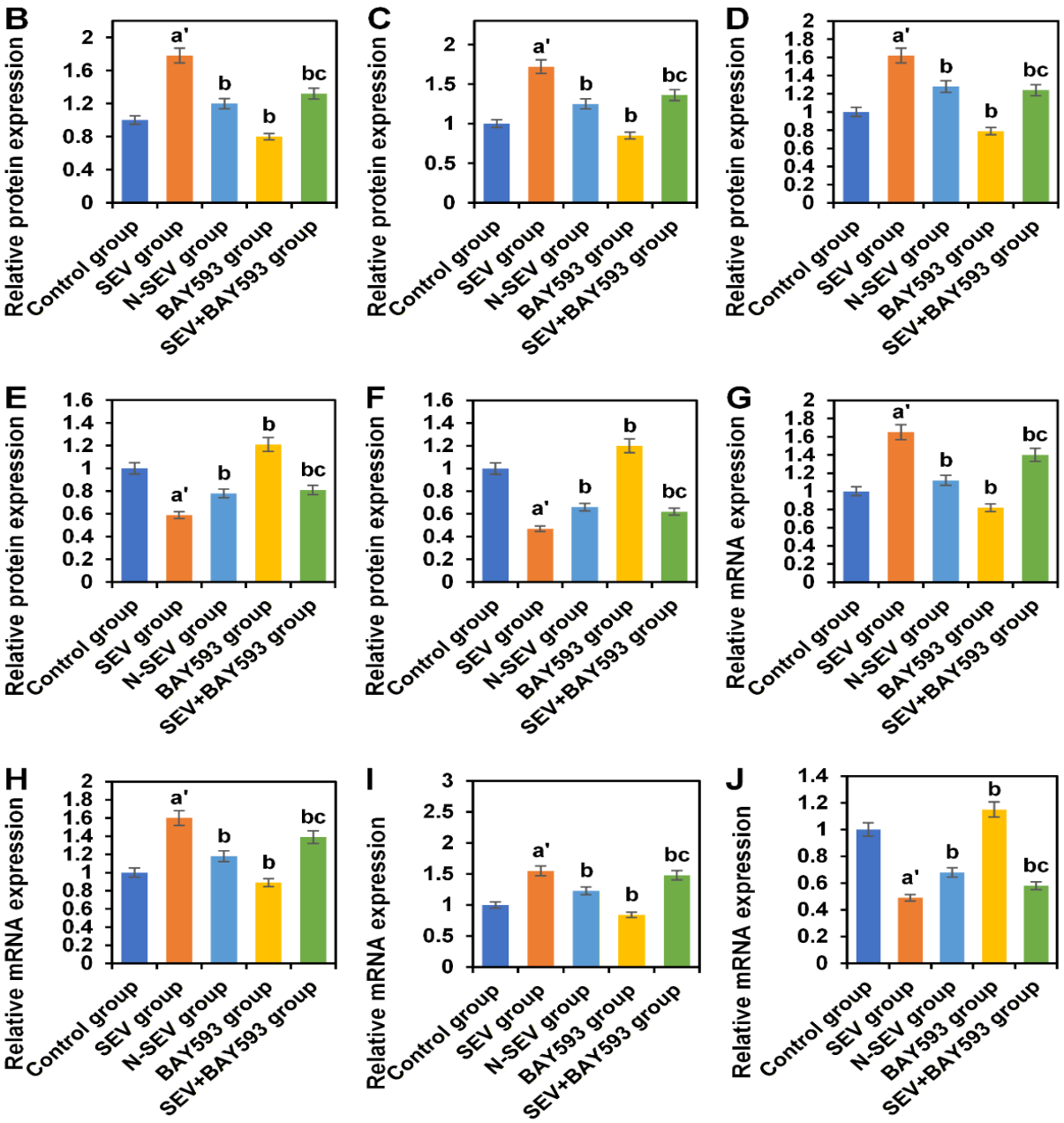


Figure 5. Evaluation results of Western Blot and qPCR for each group (mean±SD). The error line was the standard deviation. Western Blot band images (A) and relative protein expression of YAP (B), TAZ (C), Vimentin (D), p-YAP (E), E-cadherin (F), relative mRNA expression of YAP (G), TAZ (H), Vimentin (I), and E-cadherin (J). [a']*P*≤0.05 vs. Control group; [b]*P*≤0.05 vs. SEV group; [c]*P*≤0.05 vs. BAY593 group.

DISCUSSION

This study found that sevoflurane anesthesia promoted the volume growth, migratory capacity and invasive potential of tumor cells within a rat cervical cancer model, whereby its mechanism of action was closely associated with the initiation of the Hippo-YAP/TAZ signaling pathway. In addition, the blocking of this pathway partially reduced the tumour-promoting effect of sevoflurane.

The Control group exhibited a rising trend in body weight; on the other hand, the SEV, N-SEV, BAY593 and SEV+BAY593 groups all decreased, and the SEV group had the largest reduction of 10%. Interestingly, the decline in

body weight within the SEV group was markedly more pronounced relative to the N-SEV group (isoflurane anesthesia group), suggesting that sevoflurane exposure may have induced a more severe systemic stress response or disturbed host metabolic homeostasis compared with isoflurane. However, due to the lack of further studies on food intake and energy metabolism indicators, as well as related hormone levels, the specific reasons for weight loss caused by sevoflurane have not been determined. The extent of body weight decline observed in the SEV+BAY593 group was alleviated relative to the SEV group, and it was suggested that the Hippo-YAP/TAZ signalling pathway may be involved in sevoflurane-induced changes in systemic physiology. Considering that YAP/TAZ is not only linked to the promotion of cancer cell proliferation, apoptosis and metabolic reprogramming but also influences the tumor-host relationship by regulating inflammation and cellular stress processes, the restoration of body weight by BAY593 may be due to a combination of reduced tumour burden and improved host stress status, rather than a single metabolic route. Ultrasound examination shows that the size of the tumour in the SEV group is larger than that in the N-SEV and BAY593 groups ($P \leq 0.05$). The difference between the SEV and N-SEV groups is particularly noteworthy. Therefore, it can be concluded that sevoflurane promotes the development of tumours more effectively than isoflurane, and this difference may be due to different effects of the two anesthetics on the immune microenvironment of the tumour. However, it may not be due to a single reason; several factors could be involved simultaneously, such as the modification of cellular signalling under anaesthesia, inflammation, oxidative stress, and changes in the tumour microenvironment (Qi *et al.,* 2021; Sztwiertnia *et al.,* 2020; Lin *et al.,* 2025). In short, the above studies support that sevoflurane may advance cervical cancer through similar mechanisms. Conversely, the BAY593 group showed the least tumour growth; thus, the inhibition of the Hippo-YAP/TAZ pathway inhibits tumour proliferation, which is consistent with previous studies that have linked dysregulated YAP/TAZ activation to carcinogenesis (Ortega and Kim, 2021).

Based on the ELISA results, compared with the Control and N-SEV groups, the SEV group had significantly higher levels of YAP, TAZ, and Vimentin, but significantly lower levels of E-cadherin. Therefore, sevoflurane may promote the EMT pathway more strongly than isoflurane. As transcriptional co-activators, YAP/TAZ need to bind to TEAD for gene transcription; thus, the increased expression of Vimentin in the SEV group may be due to TEAD-mediated transcriptional activation. Li *et al.* (2022) demonstrated that the activation of YAP/TAZ accelerates tumour growth. Additionally, Tiron and others (2021) have reported that exposure to sevoflurane can regulate the AKT pathway and increase Vimentin expression; thus, it may facilitate the malignant phenotype of triple-negative breast cancer cells by EMT. Marked discrepancies were detected between the SEV and N-SEV groups; therefore, it further supports the notion that sevoflurane itself, rather than inhalation anesthesia as a whole, drives EMT-related molecular changes.

Both the wound healing assay and Transwell experiments consistently revealed that sevoflurane elevated the migratory and invasive capacities of cervical cancer cells compared to the Control and N-SEV groups. Therefore, sevoflurane exerts stronger effects on boosting cancer cell dissemination than isoflurane. Huang and others proposed that Sevoflurane may trigger tumour cell migration by means of cytoskeletal rearrangement and modifications in the microenvironmental structure (Huang *et al.,* 2024). Based on the confirmed feedback loop between cytoskeletal rearrangement and the Hippo pathway, sevoflurane may modulate YAP/TAZ nuclear translocation by altering the arrangement of actin filaments or focal adhesion dynamics; more research is required to verify this hypothesis. Nevertheless, research has shown that perioperative morphine exposure can promote angiogenesis in recurrent tumours after breast cancer surgery and enhance the metastatic ability of dormant tumour cells (Cheng *et al.,* 2019). Therefore, the various anaesthetics may have different effects on the development of cancer. The BAY593 group had reduced migration and invasion, so it can be concluded that blocking the Hippo-YAP/TAZ pathway restrains the dissemination of cancer cells. An increase in the activity of the Hippo-YAP/TAZ pathway facilitates tumour dissemination and metastatic progression; therefore, inhibition of this pathway has the opposite effect (Franklin *et al.,* 2023). In light of the data acquired from Western blotting and qPCR, YAP, TAZ and Vimentin showed upregulated expression within the SEV group ($P \leq 0.05$), and p-YAP together with E-cadherin were downregulated. Therefore, it has been determined that sevoflurane facilitates the migratory and invasive behaviours of cervical cancer cells via triggering the Hippo-YAP/TAZ pathway. Sevoflurane can decrease p-YAP and thus may weaken the functional status of the canonical Hippo kinase cascade (MST/LATS), but it has not been ruled out that YAP/TAZ is regulated by other non-canonical pathways, such as mechanotransduction or GPCR signalling. Previous studies have shown that aberrant activation of YAP and TAZ, the central transcriptional co-activators belonging to the Hippo signalling pathway, can promote the proliferation, EMT, invasion and distant metastasis of cancer cells, and abundant expression of these molecules frequently correlates with unfavourable clinical prognoses (Totaro *et al.,* 2018; Zanconato *et al.,* 2016; Lin *et al.,* 2023). Sevoflurane reduced E-cadherin and increased Vimentin in this study; therefore, it may promote the EMT program. Activation of the EMT program serves as a primary route for malignant cells to gain migratory capacity, and YAP/TAZ promote EMT by elevating the abundance of transcription factors such as Snail and Twist. Notably, compared with the SEV group, the SEV+BAY593 group exhibited significantly reduced levels of YAP, TAZ and Vimentin, as well as a marked elevation in E-cadherin; therefore, BAY593 appeared to partially reverse the molecular alterations caused by sevoflurane.

However, these markers in the SEV+BAY593 group were still significantly different from those in the BAY593 group; thus, the reversal is incomplete. This incomplete reversal may be due to several reasons. Initially, the dosage and administration regimen of BAY593 in this study may have been insufficient to achieve complete pathway blockade under continuous sevoflurane stimulation. Secondly, sevoflurane may promote the migratory and invasive phenotypes of tumour cells through pathways independent of, yet parallel to, the Hippo-YAP/TAZ axis, such as the PI3K/Akt, Wnt/β-catenin, or MAPK signalling cascades (Quan *et al.,* 2022; Hu *et al.,* 2021). Furthermore, mechanical signals generated by changes in the tumour microenvironment due to sevoflurane may sustain YAP/TAZ activity through mechanotransduction even in the presence of pharmacological inhibition (Lin *et al.*, 2024). These possibilities warrant systematic investigation in future studies.

In addition, this study has several limitations. First, this model does not have a full-fledged immune system and is unable to reproduce the various interactions among immune cells and tumour cells in the human tumour microenvironment. Secondly, although the immunosuppression induced by cyclophosphamide in SD rats is partially similar to the perioperative immunosuppressed state, this chemically induced immunosuppression is still significantly different from the immune status of clinical patients with cervical cancer. HeLa cells are also a human-derived cell line, and after transplantation, they cannot replicate the heterogeneity and complexity of the human tumour stroma. The single cell line was also unable to show the heterogeneity of tumours in various types of cervical cancer and among different patients (Xu *et al.,* 2019). In addition, this study has not been comprehensive enough to consider the impact of stromal components, extracellular matrix stiffness, and other mechanical signals in the tumor microenvironment on drug response (Zhang *et al.,* 2025; Wei *et al.,* 2022). Therefore, the extension of the results of this study should be done cautiously, and more clinical models need to be validated in the future. Moreover, anesthetic drugs may influence tumor volume by inhibiting angiogenesis (Wang *et al.,* 2020) or modulating immune function (Kim *et al.,* 2022; Song and Tan, 2022), but variations in experimental conditions and drug types may lead to different outcomes. Nevertheless, this study provides important clues for further exploration of the mechanisms underlying the interaction between anesthetics and tumors. Future studies should employ a broader range of cervical cancer cell lines covering different HPV types and invasive potentials, as well as more clinically relevant models such as patient-derived xenograft systems and humanized immune mouse models. Furthermore, the potential of combining sevoflurane with YAP/TAZ-targeted therapy as a novel perioperative strategy to mitigate anesthesia-related tumor promotion warrants investigation.

Conclusion: This study demonstrates that sevoflurane anesthesia enhances the migratory and invasive capacities of rat cervical carcinoma cells by activating the Hippo-YAP/TAZ signalling pathway, and the effect of sevoflurane is significantly stronger than that of isoflurane. Inhibition of this pathway partially reverses the above effects. These results have elucidated the effects of anaesthetics on the behaviour of aggressive cancer cells and provided new experimental data to optimise perioperative anaesthesia strategies for cancer patients. It also preliminarily suggests that the Hippo-YAP/TAZ pathway could serve as a promising intervention target for cervical cancer. Subsequent investigations should assess the impacts of anaesthetic agents on tumour progression by adopting models with greater clinical translational value, including patient-derived xenograft (PDX) models, and explore the feasibility of combining sevoflurane with YAP/TAZ-targeted therapy. Given the limitations of the current rat model, further validation is needed in clinical settings or humanized models.

Authors' Contributions: Mengke Fang and Shengqiang Lu designed experiments; Mengke Fang and Li Chen analyzed data; Mengke Fang and Li Chen collected samples; Mengke Fang and Shengqiang Lu performed experiments; Mengke Fang and Shengqiang Lu wrote the manuscript. All authors agreed to publish this article.

Animal rights statement: All animal experiments were approved by Ethics Committee of Hubei Cancer Hospital (Wuhan, China), in compliance with Chinese national guidelines for the care and use of animals.

Conflict of interests: None

REFERENCES

Bou Antoun, N., H. T. Afshan Mahmood, A. J. Walker, H. Modjtahedi, R. P. Grose, and A. M. Chioni (2025). Development and Characterization of Three Novel FGFR Inhibitor Resistant Cervical Cancer Cell Lines to Help Drive Cervical Cancer Research. Int J Mol Sci. 26(5): 1799. https://doi.org/10.3390/ijms26051799

Cao, Y., W. Lv, W. Ding, and J. Li (2020). Sevoflurane Inhibits the Proliferation and Invasion of Hepatocellular Carcinoma Cells Through Regulating the PTEN/Akt/GSK-3β/β-Catenin Signaling Pathway by Downregulating miR-25-3p. Int J Mol Med. 46(1): 97-106. https://doi.org/10.3892/ijmm.2020.4577

Cheng, S., M. Guo, Z. Liu, Y. Fu, H. Wu, C. Wang, and M. Cao (2019). Morphine Promotes the Angiogenesis of Postoperative Recurrent Tumors and Metastasis of Dormant Breast Cancer Cells. Pharmacology. 104(5-6): 276-286. https://doi.org/10.1159/000502107

Chen, M., L. Zhou, Z. Liao, X. Ye, X. Xuan, B. Gu, and F. Lu. (2019). Sevoflurane Inhibited Osteosarcoma Cell Proliferation And Invasion Via Targeting miR-203/WNT2B/Wnt/β-Catenin Axis. Cancer Manag Res. 11: 9505-9515. https://doi.org/10.2147/CMAR.S225911

Choi, H. S., H. J. Jang, M. K. Kristensen, and T. H. Kwon (2024). TAZ Is Involved in Breast Cancer Cell Migration via Regulating Actin Dynamics. Front Oncol. 14: 1376831. https://doi.org/10.3389/fonc.2024.1376831

Das, S., A. Babu, T. Medha, G. Ramanathan, A. G. Mukherjee, U. R. Wanjari, R. Murali, S. Kannampuzha, A. V. Gopalakrishnan, K. Renu, D. Sinha, and C. George Priya Doss (2023). Molecular Mechanisms Augmenting Resistance to Current Therapies in Clinics Among Cervical Cancer Patients. Med Oncol. 40(5): 149. https://doi.org/10.1007/s12032-023-01997-9

Fan, S., T. Price, W. Huang, M. Plue, J. Warren, P. Sundaramoorthy, B. Paul, D. Feinberg, N. MacIver, N. Chao, D. Sipkins, and Y. Kang (2020). PINK1-Dependent Mitophagy Regulates the Migration and Homing of Multiple Myeloma Cells via the MOB1B-Mediated Hippo-YAP/TAZ Pathway. Adv Sci. 7(5): 1900860. https://doi.org/10.1002/advs.201900860

Franklin, J. M., Z. Wu, and K. L. Guan, (2023). Insights into recent findings and clinical application of YAP and TAZ in cancer. Nat Rev Cancer. 23(8): 512-525. https://doi.org/10.1038/s41568-023-00579-1

Huang, X., X. Lao, C. He, J. Wang, and Y. Pan (2024). The Mechanism of Sevoflurane Affecting Ovarian Cancer Cell Proliferation and Migration by Regulating RNA Methylase TRDMT1 to Activate the β-Catenin Pathway. Cell Biol Toxicol. 40(1): 108. https://doi.org/10.1007/s10565-024-09941-x

Hu, N., J. A. Duan, Y. Yu, D. Li, J. Chen, and H. Yan (2021). Sevoflurane Inhibits the Migration, Invasion and Induces Apoptosis by Regulating the Expression of WNT1 via miR-637 in Colorectal Cancer. Anticancer Drugs. 32(5): 537-547. https://doi.org/10.1097/CAD.0000000000001061

Hu, Z., Q. Jia, S. Yao, and X. Chen (2024). The TWIK-related acid sensitive potassium 3 (TASK-3) channel contributes to the different effects of anesthetics on the growth and metastasis of ovarian cancer cells. Heliyon. 10(15): e34973. https://doi.org/10.1016/j.heliyon.2024.e34973

Ishikawa, M., M. Iwasaki, H. Zhao, J. Saito, C. Hu, Q. Sun, A. Sakamoto, and D. Ma (2021). Inhalational Anesthetics Inhibit Neuroglioma Cell Proliferation and Migration via miR-138, -210 and -335. Int J Mol Sci. 22(9): 4355. https://doi.org/10.3390/ijms22094355

Kim, R., A. Kawai, M. Wakisaka, and T. Kin (2022). Current Status and Prospects of Anesthesia and Breast Cancer: Does Anesthetic Technique Affect Recurrence and Survival Rates in Breast Cancer Surgery?. Front Oncol. 12: 795864. https://doi.org/10.3389/fonc.2022.795864

Li, H., B. K. Wu, M. Kanchwala, J. Cai, L. Wang, C. Xing, Y. Zheng, and D. Pan (2022). YAP/TAZ drives cell proliferation and tumour growth via a polyamine-eIF5A hypusination-LSD1 axis. Nat Cell Biol. 24(3): 373-383. https://doi.org/10.1038/s41556-022-00848-5

Lin, L., L. Kong, X. Dong, and S. Ma (2025). Sevoflurane Suppresses Growth and Metastasis of Bladder Cancer Cells via Inducing Ferroptosis and Antitumor Microenvironment Through Akt/mTOR/SREBP1 Signaling. Chem Biol Interact. 421: 111766. https://doi.org/10.1016/j.cbi.2025.111766

Lin, W. H., L. M. Cooper, and P. Z. Anastasiadis (2023). Cadherins and Catenins in Cancer: Connecting Cancer Pathways and Tumor Microenvironment. Front Cell Dev Biol. 11: 1137013. https://doi.org/10.3389/fcell.2023.1137013

Novikov, N. M., S. Y. Zolotaryova, A. M. Gautreau, and E. V. Denisov (2021). Mutational Drivers of Cancer Cell Migration and Invasion. Br J Cancer. 124(1): 102-114. https://doi.org/10.1038/s41416-020-01149-0

Pan, D. (2022). The Unfolding of the Hippo Signaling Pathway. Dev Biol. 487: 1-9. https://doi.org/10.1016/j.ydbio.2022.04.001

Qi, Y., L. Guo, Y. Liu, T. Zhao, X. Liu, and Y. Zhang (2021). Sevoflurane Limits Glioma Progression by Regulating Cell Proliferation, Apoptosis, Migration, and Invasion via miR-218-5p/DEK/β-Catenin Axis in Glioma. Cancer Manag Res. 13: 2057-2069. https://doi.org/10.2147/CMAR.S265356

Quan, Y., S. Li, Y. Wang, G. Liu, Z. Lv, and Z. Wang (2022). Propofol and Sevoflurane Alleviate Malignant Biological Behavior and Cisplatin Resistance of Xuanwei Lung Adenocarcinoma by Modulating the Wnt/β-Catenin Pathway and PI3K/AKT Pathway. Anticancer Agents Med Chem. 22(11): 2098-2108. https://doi.org/10.2174/1871520621666211026092405

Song, Z., and J. Tan (2022). Effects of Anesthesia and Anesthetic Techniques on Metastasis of Lung Cancers: A Narrative Review. Cancer Manag Res. 14: 189-204. https://doi.org/10.2147/CMAR.S343772

Sztwiertnia, I., J. Schenz, K. Bomans, D. Schaack, J. Ohnesorge, S. Tamulyte, M. A. Weigand, and F. Uhle (2020). Sevoflurane Depletes Macrophages from the Melanoma Microenvironment. PLoS One. 15(5): e0233789. https://doi.org/10.1371/journal.pone.0233789

Tiron, C. E., E. Patrașcanu, P. A. Postu, I. C. Vacarean Trandafir, A. Tiron, and I. Grigoras (2021). Sevoflurane Modulates AKT Sevforms in Triple Negative Breast Cancer Cells. An Experimental Study. Curr Issues Mol Biol. 43(1): 264-275. https://doi.org/10.3390/cimb43010022

Totaro, A., T. Panciera, and S. Piccolo (2018). YAP/TAZ Upstream Signals and Downstream Responses. Nat Cell Biol. 20(8): 888-899. https://doi.org/10.1038/s41556-018-0142-z

Wang, X., Y. Yao, and J. Gao (2020). Sevoflurane Inhibits Growth Factor-Induced Angiogenesis Through Suppressing Rac1/Paxillin/FAK and Ras/Akt/mTOR. Future Oncol. 16(22): 1619-1627. https://doi.org/10.2217/fon-2020-0221

Wei, J., J. Yao, M. Yan, Y. Xie, P. Liu, Y. Mao, and X. Li (2022). The Role of Matrix Stiffness in Cancer Stromal Cell Fate and Targeting Therapeutic Strategies. Acta Biomater. 150: 34-47. https://doi.org/10.1016/j.actbio.2022.08.005

Xu, C., X. Li, P. Liu, M. Li, and F. Luo (2019). Patient-derived xenograft mouse models: A high fidelity tool for individualized medicine. Oncol Lett. 17(1): 3-10. https://doi.org/10.3892/ol.2018.9583

Yang, N. S., W. J. Zhong, H. X. Sha, C. Y. Zhang, L. Jin, J. X. Duan, J. B. Xiong, Z. J. You, Y. Zhou, and C. X. Guan (2024). mtDNA-cGAS-STING Axis-Dependent NLRP3 Inflammasome Activation Contributes to Postoperative Cognitive Dysfunction Induced by Sevoflurane in Mice. Int J Biol Sci. 20(5): 1927-1946. https://doi.org/10.7150/ijbs.91543

Zaman, M. S., N. Chauhan, M. M. Yallapu, R. K. Gara, D. M. Maher, S. Kumari, M. Sikander, S. Khan, N. Zafar, M. Jaggi, and S. C. Chauhan (2016). Curcumin Nanoformulation for Cervical Cancer Treatment. Sci Rep. 6: 20051. https://doi.org/10.1038/srep20051

Zanconato, F., M. Cordenonsi, and S. Piccolo (2016). YAP/TAZ at the Roots of Cancer. Cancer Cell. 29(6): 783-803. https://doi.org/10.1016/j.ccell.2016.05.005

Zhang, M., and B. Zhang (2025). Extracellular Matrix Stiffness: Mechanisms in Tumor Progression and Therapeutic Potential in Cancer. Exp Hematol Oncol. 14(1): 54. https://doi.org/10.1186/s40164-025-00647-2

Zhou, T., X. Li, J. Liu, and J. Hao (2023). The Hippo/YAP Signaling Pathway: The Driver of Cancer Metastasis. Cancer Biol Med. 20(7): 483–9. https://doi.org/10.20892/j.issn.2095-3941.2023.0164